Journal of Solid State Chemistry 200 (2013) 157–164

Contents lists available at SciVerse ScienceDirect

Journal of Solid State Chemistry

journal homepage: www.elsevier.com/locate/jssc

# Crystal structure and phase transition mechanisms in $CsFe_2F_6$

M.S. Molokeev [a,*,1], E.V. Bogdanov [a,b], S.V. Misyul [c], A. Tressaud [d], I.N. Flerov [a,c]

[a] Kirensky Institute of Physics, Siberian Department RAS, 660036 Krasnoyarsk, Russia
[b] Institute of Energetics and Management of Energetic Sources, State Agrarian University, 660049 Krasnoyarsk, Russia
[c] Institute of Physical Engineering and Radioelectronics, Siberian Federal University, 660074 Krasnoyarsk, Russia
[d] Institute of Condensed Matter Chemistry of Bordeaux (ICMCB-CNRS), Université Bordeaux, 33608-Pessac, France

ARTICLE INFO

*Article history:*
Received 25 October 2012
Received in revised form
22 January 2013
Accepted 22 January 2013
Available online 31 January 2013

*Keywords:*
Phase transitions
Iron fluorides
Defect pyrochlore

ABSTRACT

For the first time, structural phase transitions induced by the temperature were found in $A_xM^{II}_xM^{III}_{(1-x)}F_3$ fluorides with the defect pyrochlore structure ($Fd\bar{3}m$, $Z=8$). The room temperature structure of $CsFe_2F_6$ was determined using X-ray powder diffraction technique. This phase was found to be ordered with the *Pnma* space group. The study of the temperature stability of orthorhombic structure by differential scanning calorimeter between 100 K and 700 K has shown a succession of phase transitions. The *Pnma* ($Z=4$)→*Imma* ($Z=4$)→$I4_1/amd$ ($Z=4$)→$Fd\bar{3}m$ ($Z=8$) structural sequence was proposed to occur within a rather narrow temperature range 500–560 K. The mechanism of structural transition has been mainly associated with the rotation of ($MF_6$) octahedra and small displacements of some Fe atoms. This assumption is in good agreement with the low experimental entropy value, which is characteristic for displacive transformations.



## 1. Introduction

Fluorides with octahedral ($MF_6$) species are known for their ability to form a lot of compounds having three-dimensional crystal structures: perovskite, elpasolite, cryolite, antifluorite, pyrochlore, etc. [1–8]. Many of them exhibit interesting physical properties such as ferromagnetic, ferroelectric, ferroelastic, as well as multiferroic.

Successive or unique structural phase transitions of displacive or order–disorder type were often observed in series of perovskite-related compounds with general formulations: $AMF_3$ (sp. gr. $Pm\bar{3}m$), $A_2MF_6$, $A_2A'MF_6$ and $A_3MF_6$ (sp. gr. $Fm\bar{3}m$) [2,9]. The temperature of structural phase transformation from the initial cubic phase depends significantly on the composition of fluorides and may lie below or above room temperature.

Another series of fluorides containing transition elements at two different oxidation states: $A_xM^{II}_xM^{III}_{(1-x)}F_3$ and $A_xM^{II}_xM'^{III}_{(1-x)}F_3$ $A_xM^{II}(M')^{III}F_3$, which is rich of representatives, is also formed by the octahedral polyhedra linked to each other by common vertices. Depending on the A cation concentration and combination of the $M^{II}$ and $(M')^{III}$ central atoms, these compounds can exhibit the structures of tetragonal- or hexagonal tungsten bronze (TTB or HTB), as well as cubic or distorted pyrochlore [4,5,7,10–12]. It was found that the most typical behaviour of such compounds is associated with the appearance of an antiferromagnetic state at low temperatures. Sometimes, as for $K_{0.6}Fe^{II}_{0.6}Fe^{III}_{0.4}F_3$ having a TTB structure at high temperature, ferroelectric, ferroelastic, charge ordered, and ferromagnetic phases can be successively realized due to transformations on cooling [13,14]. There is no example so far of a structural phase transition induced by temperature change in any $A_xM^{II}_xM^{III}_{(1-x)}F_3$ and $A_xM^{II}_xM'^{III}_{(1-x)}F_3$ compounds, into or from the cubic pyrochlore structure. It is rather surprising, because many different fluorides containing $M^{II}/M^{III}$ combination, especially at $x=0.5$, reveal at room temperature individual symmetries connected by a group-to-subgroup relation $Fd\bar{3}m$→*Imma*→*Pnma*→$P2_1/c$ [15].

On the other hand, a very interesting phenomenon was observed for $KNiCrF_6$ that maintains a $Fd\bar{3}m$ symmetry at ambient pressure till the melting point (1200 °C) [16]. After one hour exposure at 800 °C under 30 kbar high pressure, this cubic structure was transformed into a TTB structure ($P4/mbm$). It was supposed that a cubic phase is metastable, because the procedure above was followed by strong decrease of the formula unit volume from 134.2 $A^3$ down to 120.0 $A^3$.

An existence of two different phases for $NH_4CoAlF_6$ was observed depending on the method of preparation [17]. Ordered structure with the *Pnma* symmetry was obtained by hydrothermal synthesis at 400 °C under 3 kbar external pressure for 2 days. Synthesis by thermal decomposition of $(NH_3)_6CoAlF_6$ led to the

* Corresponding author. Fax: +7 3912 43 89 23.
*E-mail addresses:* msmolokeev@gmail.com (M.S. Molokeev), evbogdanov@iph.krasn.ru (E.V. Bogdanov), misjul@akadem.ru (S.V. Misyul), tressaud@icmcb-bordeaux.cnrs.fr (A. Tressaud), flerov@iph.krasn.ru (I.N. Flerov).
[1] postal address: Kirensky Institute of Physics, Akademgorodok 50, build. 38, 660036 Krasnoyarsk, Russia.

0022-4596/$ - see front matter © 2013 Elsevier Inc. All rights reserved.
http://dx.doi.org/10.1016/j.jssc.2013.01.038

formation of a cubic structure (sp. gr. $Fd\bar{3}m$) with a disorder of Co and Al atoms in the octahedral sites. In this case too, the cubic phase was found to be metastable. Prolonged heating at 350 °C (about one week) led to its conversion into an orthorhombic phase.

In the $A_xFe^{II}_xFe^{III}_{(1-x)}F_3$ series, with *A*: Li, Na, K, Rb, Cs, Tl, $NH_4$, the defect pyrochlore cubic structure at room temperature was not observed [10]. Substitution of the monovalent cation and variation of its concentration or, in other words, changing the chemical pressure, led to stabilize different phases at ambient conditions. In the $FeF_3$–$AFeF_3$ phase diagrams with *A*: K, Rb, Cs, Tl, $NH_4$ an orthorhombic phase was found to be stable at room temperature in rather narrow ranges of *x* values, close to 0.5. The symmetry of the $NH_4Fe_2F_6$ single crystal prepared by hydrothermal synthesis (at 350 °C and 2.35 kbar) was refined in the *Pnma* sp. gr., with an ordering of the Fe cations [18]. Recently, the same space group was found for the room temperature structure of $RbFe_2F_6$, which did not undergo any structural phase transitions down to 4 K, in accordance with neutron diffraction data [19]. High temperature differential thermal analysis did not reveal any peculiarities up 350 °C, at which temperature the compound was decomposed. The results obtained in [18,19] are in contradiction with the space group *Imma* suggested previously without any certainty for $CsFe_2F_6$ [20].

Taking into account the information above, we have reinvestigated in the present paper the room temperature structure of $CsFe_2F_6$ using X-ray powder diffraction technique. This phase was found to be ordered with the *Pnma* space group. The study of the temperature stability of orthorhombic structure by differential scanning calorimeter between 100 K and 700 K has shown the succession of phase transitions in rather narrow temperature range 500–560 K.

## 2. Experimental

$CsFe_2F_6$ was synthesized using solid state procedures as developed in [1]. Starting fluorides CsF, $FeF_2$ and $FeF_3$ were mixed in stoichiometric amounts and carefully ground in a glove box containing less than 3 ppm of $H_2O$ and $O_2$. $FeF_2$ was prepared by fluorination of $FeCl_2$ under a stream of anhydrous HF at 400 °C for several hours, whereas $FeF_3$ was obtained by fluorination of $FeCl_3$ in pure $F_2$ atmosphere at 300 °C for several hours. CsF was thoroughly dehydrated before use. Single-crystals of $CsFe_2F_6$ in the size of several $mm^3$ in volume were grown by heating the stoichiometric mixture in a sealed platinum crucible. The crucible was heated to 750 °C and the temperature was decreased down 550 °C at 5 °C/h, and then the heating was stopped.

Because $CsFe_2F_6$ single-crystals have multiply twins at room temperature, the powder X-ray diffraction (XRD) data were collected on Bruker D8 ADVANCE Bragg-Brentano diffractometer with linear detector VANTEC using Cu-$K\alpha$ radiation. The beam was controlled by the 0.6 mm fixed divergence slit, 6 mm receiving VANTEC slit and Soller slits. An attachment Anton Paar TTK450 was used for low- and high-temperature measurements.

The variable counting time (VCT) and step size (VSS) scheme were used to collect the diffraction data. The measurement time was systematically increased towards higher $2\theta$ angles, leading to drastically improved data quality [21–23]. As a rule, 5–8 data points should be measured over the full-width-at-half-maximum. However, peaks are significantly broadened for increasing $2\theta$. Therefore, for high $2\theta$ angles, the step size should be increased to avoid wasting measurement time [24].

To collect the X-ray data at 298 K using VCT scheme, four ranges were generated on the diffraction pattern (Fig. 1). Total experimental time was equal to 30 h.

The chosen $2\theta$ ranges for structure determination were the same at 133 K and 573 K (Fig. 2) but time per step was reduced by 5. To get information on the temperature dependence of the unit cell parameters, 17 and 36 X-ray patterns were collected from 133 K to 293 K and from 303 K to 613 K, respectively. Total experimental time was equal to 36 min for each experiment.

Thirteen X-ray patterns were measured from 471 K to 567 K in a narrow $2\theta$ range: 26.8–29.2° (step size 0.016, 5 s per step), in order to evidence possible symmetry distortion at phase transitions, characterized by peak splitting and/or appearance of superstructure peak. The XRD Wizard [24] was used to generate VCT/VSS ranges for experiments. Peak positions were determined with the program EVA (2004 release), available in the PC software package DIFFRAC-PLUS supplied from Bruker.

The thermal stability of the room temperature phase of $CsFe_2F_6$ was examined by heat capacity study. The measurements were performed with a differential scanning microcalorimeter DSM-10M working between 100 K and 700 K. The powdered sample prepared from the single crystals was put in an aluminum sample holder. Experiments were carried out on several samples

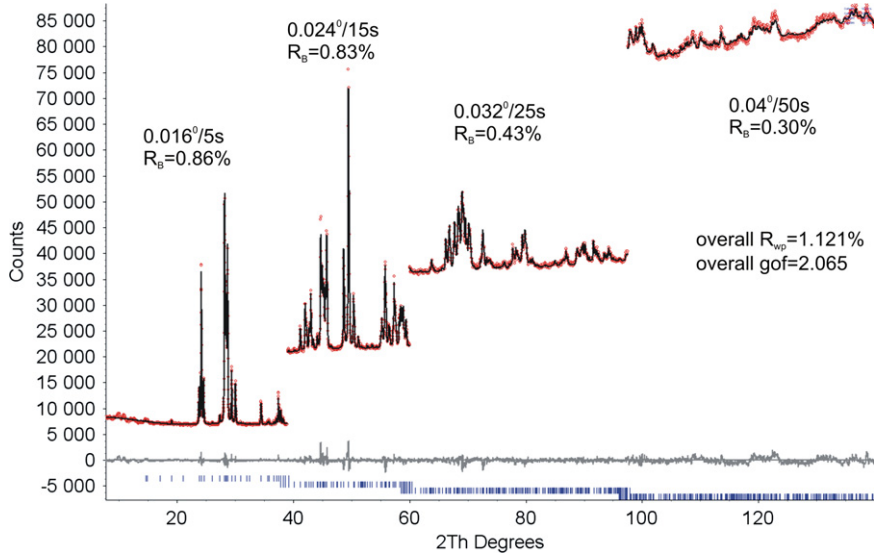


**Fig. 1.** Rietveld difference plot to count/step data of low-temperature phase and Bragg *R*-factors of $CsFe_2F_6$ at 298 K.

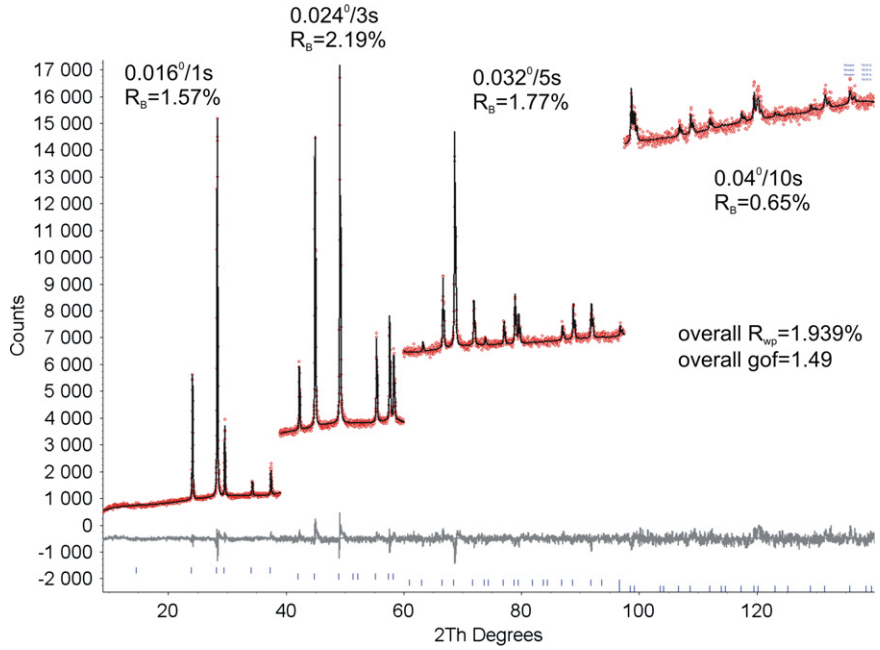


**Fig. 2.** Rietveld difference plot to count/step data and Bragg *R*-factors of high-temperature phase of $CsFe_2F_6$ at 573 K.

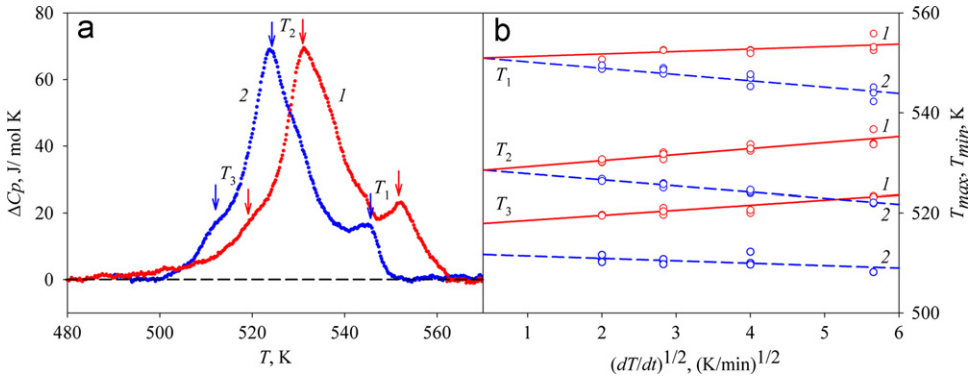


**Fig. 3.** (a) Temperature dependence of the excess heat capacity on heating (1) and cooling (2) with a 16 K/min rate. (b) Dependence of the phase transition temperatures on the $dT/dt$ value on heating ($1-T_{max}$) and on cooling ($2-T_{min}$).

with the mass of about 0.01–0.03 g in repeated heating–cooling cycles. The rate of temperature change $dT/dt$ ranged from 4 K/min to 32 K/min, to reveal the real hysteretic phenomena. In the first stage, the heat flow through the sample and reference compound was recorded against temperature. Then, after elimination of background, the information on excess heat capacity $\Delta C_p$ connected with the phase transitions was obtained.

## 3. Results

X-ray structural characterization of $CsFe_2F_6$ at room temperature has shown that crystals produced are free from any addition or impurity. The main structural reflections were found to coincide with the orthorhombic syngony suggested in [20]. But our diffraction pattern in 133–517 K temperature range is not consistent with this body centered orthorhombic structure due to the presence of $hkl$ $h+k+l\neq 2n$ reflections, e.g., 2 1 0. As it will be seen below, the detailed analysis of the temperature dependence of the XRD patterns proves the validity of such a hypothesis.

### 3.1. Calorimetric study

The calorimetric measurements did not show any anomalous behavior of the heat capacity $Cp(T)$ below room temperature down to 100 K. Taking into account the preparation temperature of crystals under study, high temperature studies were performed until 700 K. In Fig. 3a, one can see that on heating with a $dT/dt=16$ K/min rate, two rather large peaks were observed on temperature dependence of $\Delta C_p$, with maxima at about 530 K and 550 K. The former anomaly was moreover accompanied by small shoulder at 520 K. On cooling, all anomalies were detected too and characterized by the temperature hysteresis with the values close to $\delta T_i \approx 10$ K. A rather good agreement was found for the phase transition temperatures and values of their hysteresis for different samples, as well as in repeated heating–cooling cycles. In the temperature range investigated, no weight losses of the samples were observed.

We have also examined the dependence of the phase transition temperatures and $\delta T_i$ values on the rate of thermal cycling (Fig. 3b). Lower $dT/dt$ value leads to the diminution of the thermal hysteresis and heat capacity anomalies. It was found

that extrapolation of $T_i(dT/dt)^{0.5}$ linear dependences to $dT/dt=0$ gives following parameters: $T_1=551\pm1$ K, $\delta T_1\geq 0$ K; $T_2=529\pm1$ K, $\delta T_2\geq 0$ K; $T_3=517\pm3$ K, $\delta T_3\approx 6$ K. These results mean that two high temperature phase transitions of the first order are close to the tricritical point, whereas at $T_3$ there is a strong first order transformation. Because of the closeness of all heat capacity anomalies, we were able to determine only the total enthalpy change associated with the succession of transformations $\Sigma\Delta H_i=\Delta H_1+\Delta H_2+\Delta H_3=1400\pm500$ J/mol. The rather high value of the error is due to the change of $\Sigma\Delta H_i$ from sample to sample.

In order to be certain that the heat capacity anomalies are associated with structural transformations, powder XRD measurements were performed on $CsFe_2F_6$ in a wide temperature range.

### 3.2. Determination of crystal structures at T=573 K and T=298 K

The cell parameters and space groups of high and low-temperature phases were found using DASH 3.3 program [25].

The analysis has shown that at 573 K the crystal structure is cubic with $a=10.51$ Å. The four best extinction symbols are presented in Table 1. So, likely the space group of the high-temperature phase is $Fd\bar{3}m$ or $Fd\bar{3}$. It was decided to use space group $Fd\bar{3}m$ because high-temperature phase of $CsFe_2F_6$ appear to be relative to pyrochlore-type structure found earlier for some fluorides $A_xM^{II}(M')^{III}F_3$ [4,8]. The program TOPAS 4.2 [26] was used to solve and refine crystal structure using simulated annealing procedure applied to the randomized coordinates of one Cs, one Fe and one F ions. Refinement with isotropic Cs, Fe and F approach was stable and gave low values of $R_B$-factor for all four regions of diffraction data (Fig. 2). So it was assumed that $Fd\bar{3}m$ space group was the right one. Main parameters of refinement are shown in Table 2. Further details of the crystal structure may be obtained from Fachinformationszentrum Karlsruhe; e-mail: crystdata@fiz-karlsruhe.de, http://www.fiz-karlsruhe.de/request_for_deposited_data.html on quoting 425260 CSD number.

**Table 1**
Most probable extinction symbols of $CsFe_2F_6$ at 573 K and 298 K obtained by DASH.

| T=573 K, cubic | | T=298 K, orthorhombic | |
|---|---|---|---|
| Extinction symbol | Log-probability | Extinction symbol | Log-probability |
| {F d – –} | 181.6 | {I – – (ab)} | 72.4 |
| {F $4_1$ – –} | 174.6 | {I – – –} | 64.7 |
| {F – – –} | 170.7 | {P n n a} | 44.7 |
| {P a – –} | 74.14 | {P n n b} | 40.9 |
| | | {P n – a} | 36.6 |
| | | {P n n n} | 35.5 |
| | | {P n n –} | 33.6 |
| | | {P – n a} | 28.1 |

**Table 2**
Main refinement parameters.

| Space group | T=573 K $Fd\bar{3}m$ | T=298 K *Pnma* |
|---|---|---|
| $a_i$ (Å) | $a_{cub}$, 10.51820(13) | $a_{orth}$, 7.2443(1) |
| $b_i$ (Å) | | $b_{orth}$, 7.48230(9) |
| $c_i$ (Å) | | $c_{orth}$, 10.4238(1) |
| $V$ (Å$^3$) | 1163.7(4) | 565.01(1) |
| $Z$ | 8 | 4 |
| $2\theta$-interval, ° | 5–140 | 5–140 |
| Number of reflections | 71 | 577 |
| Number of parameters of refinement | 17 | 29 |
| $R_{wp}$, % | 1.939 | 1.121 |

For low temperature phase (Fig. 1) the program DASH 3.3 led to the orthorhombic cell $a=7.238$ Å; $b=7.4757$ Å; $c=10.4200$ Å ($M(39)=19.1$, $F(39)=39.9$). Space group determination using 26 peaks ranging between 5° and 42° revealed 8 best extinction symbols in Table 1. However diffraction patterns in Fig. 4 and Fig. 5a showed at $T=298$ K the presence of $(2\,1\,0)_{orth}$ and $(3\,0\,2)_{orth}$ reflections (here and further: orth—orthorhombic cell; cub—cubic cell). Both or one of them must disappear for all these extinction symbols, excluding {*P n – a*}. So, from most probable extinction symbols remain {*P n – a*} and corresponding space group is *Pnma*.

To get even more evidence in the validity of the sp. gr. we decided to use homology method [27] and tools ISODISTORT [28]/ISOTROPY [29] admitting to generate, explore and visualize distortion modes induced by irreducible representations of the parent space-group symmetry.

Comparison of XRPD data collected at 298 K with those collected at 573 K indicated that a change in structure had occurred e.g., $(2\,2\,0)_{cub}$ reflection had split into three peaks with intensities in the ratio 1:4:1 (Fig. 4), the $(2\,2\,2)_{cub}$ had split into two peaks in the ratio 1:1. These reflections could be indexed by the related orthorhombic cell $a_{cub}/\sqrt{2}\times a_{cub}/\sqrt{2}\times a_{cub}$ (or basis vectors (½ ½ 0, ½ –½ 0, 0 0 1). Superstructure peaks $(2\,1\,0)_{orth}$, $(3\,0\,2)_{orth}$ imply primitive orthorhombic cell. Subgroups of $Fd\bar{3}\ m$ consistent with this cell size and centering were explored using the web-based ISODISTORT software. Fourteen possible structures were considered, which allow cation displacements, anion displacements and $Fe^{II}/Fe^{III}$ ordering (Table 3).

Cells 2, 3, 9, 11 have extinction rules which do not satisfy our experimental observations of superstructure. So, the list can be reduced to only two centrosymmetric subgroups (*Pmma*, *Pnma*) and eight non-centrosymmetric. It is obvious that first of all we should try to find structure in centrosymmetric space groups. One of them, *Pnma*, is ideally suitable in our case for two reasons: (i) DASH 3.3 points this space group as the most probable one; (ii) several $CsM^{II}M^{III}F_6$ pyrochlore-like compounds exhibit this space group [15,30,31].

The crystal structure of the low-temperature phase at $T=298$ K was solved by a distortion-mode refinement of X-ray data using TOPAS 4.2 program, with file generated by ISODISPLACE. Space group *Pnma* was used. There are four order parameters associated with all displacements of atoms: *GM*1+(*a*); *GM*3+(*b*,0); *GM*5+($\xi$,0,0); *X*4($\eta$,0,0,0,0,0). *GM*1+ and *GM*3+ acts on 48*f* sites occupied by *F*, *GM*5+ acts on *F* sites and *Cs* sites. *GM*5+ shifts atom *Cs* along $c_{orth}$ and orders $Fe^{II}/Fe^{III}$. *X*4 acts on all sites. *X*4 shifts atom *Cs* along $a_{orth}$. All corresponded amplitudes were used to find model of structure by simulated anneal method. Then coordinates and isotropic thermal parameters of all atoms were refined independently by the Rietveld method. The refinement yielded satisfactory final *R*-factors (Fig. 2, Table 2), interatomic distances as well as thermal parameters. Coordinates of atoms and their isotropic thermal parameters of low-temperature phase at $T=298$ K are presented in Table 4 and main bond lengths in Table 5. Further details of the crystal structure may be obtained from Fachinformationszentrum Karlsruhe; e-mail: crystdata@fiz-karlsruhe.de, http://www.fiz-karlsruhe.de/request_for_deposited_data.html on quoting 425261 CSD number.

Complete mode details after mode decomposition of distorted structure at 298 K in ISODISTORT show the following displacive mode amplitudes: *GM*1+ all 0.068(18); *GM*3+ all 0.210(17); *GM*5+ all 0.645(19); *X*4 all 1.830(19). It is obvious that order parameter ($\eta$,0,0,0,0,0) of *X*4 irreducible representation (irrep.) is critical.

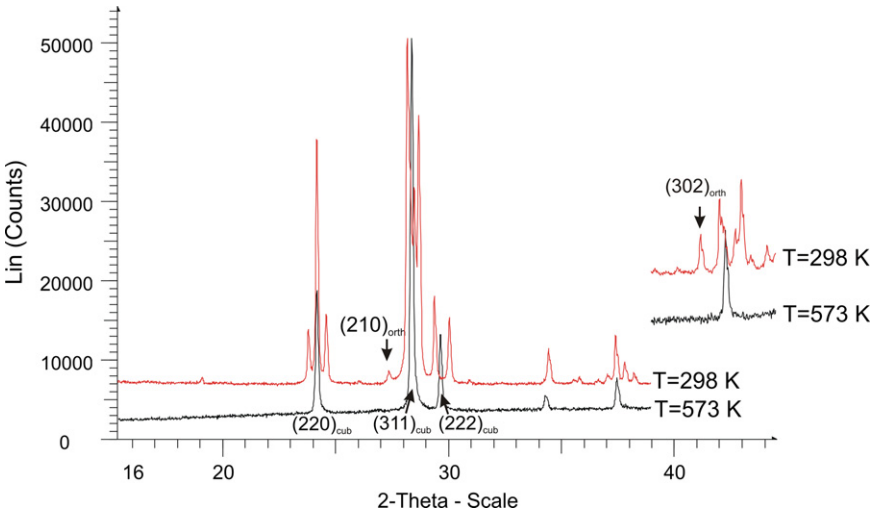


**Fig. 4.** XRD pattern of $CsFe_2F_6$ at 298 K (top pattern) and 573 K (bottom pattern). One can see at $T=298$ K two superstructure reflections $(2\,1\,0)_{orth}$ and $(3\,0\,2)_{orth}$ and the splitting of the main cubic reflections $(2\,2\,0)_{cub}$, $(3\,1\,1)_{cub}$, $(2\,2\,2)_{cub}$.

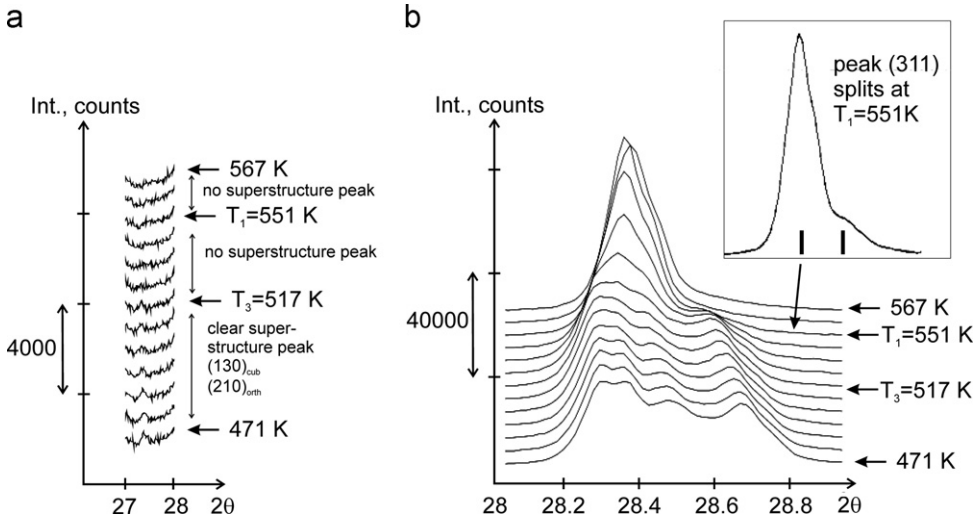


**Fig. 5.** (a) Appearance of superstructure reflections on cooling. (b) Splitting of the main (3 1 1) reflection on cooling.

**Table 3**
Full list of subgroups of $Fd\bar{3}m$ space group with orthorhombic primitive cells and minimal s which probably can satisfy our experimental data.

| *N* | Space group | Possible sets of primary order param. | Basis, origin | *s* |
|---|---|---|---|---|
| 1 | *Pmma* | *X*1 | {(0,1/2,1/2),(0,−1/2,1/2),(1,0,0)}, origin=(0,0,0) | 2 |
| 2 | *Pnna* | *X*2 | {(0,1/2,1/2),(0,−1/2,1/2),(1,0,0)}, origin=(0,0,0) | 2 |
| 3 | *Pmna* | *X*3 | {(0,−1/2,1/2),(0,1/2,1/2),(−1,0,0)}, origin=(0,0,0) | 2 |
| 4 | *Pnma* | *X*4 | {(0,−1/2,1/2),(0,1/2,1/2),(−1,0,0)}, origin=(0,0,0) | 2 |
| 5 | *Pmm*2 | *X*1 | {(0,−1/2,1/2),(0,1/2,1/2),(−1,0,0)}, origin=(0,1/8,1/8) | 2 |
| 6 | $Pmc2_1$ | *GM*4-*X*1 | {(0,1/2,1/2),(−1,0,0),(0,−1/2,1/2)}, origin=(−1/4,1/8,1/8) | 2 |
| 7 | *Pma*2 | *GM*4-*X*1 | {(0,1/2,1/2),(−1,0,0),(0,-1/2,1/2)}, origin=(0,0,0) | 2 |
| 8 | *Pnc*2 | *GM*4-*X*2 | {(0,1/2,1/2),(−1,0,0),(0,−1/2,1/2)}, origin=(0,0,0) | 2 |
| 9 | $Pmn2_1$ | *GM*2-*X*3 | {(0,-1/2,1/2),(0,1/2,1/2),(−1,0,0)}, origin=(0,0,0) | 2 |
| 10 | $Pna2_1$ | *GM*4-*X*2 | {(0,1/2,1/2),(−1,0,0),(0,−1/2,1/2)}, origin=(−1/4,1/8,1/8) | 2 |
| 11 | *Pnn*2 | *X*2 | {(0,−1/2,1/2),(0,1/2,1/2),(−1,0,0)}, origin=(0,1/8,1/8) | 2 |
| 12 | $P222_1$ | *GM*3-*X*1 | {(−1,0,0),(0,−1/2,1/2),(0,1/2,1/2)}, origin=(0,1/8,1/8) | 2 |
| 13 | $P222_1$ | *X*3 | {(0,−1/2,1/2),(0,1/2,1/2),(−1,0,0)}, origin=(0,−1/8,1/8) | 2 |
| 14 | $P2_12_12_1$ | *X*4 | {(1,0,0),(0,1/2,1/2),(0,-1/2,1/2)}, origin=(0,0,1/4) | 2 |

*s*—multiplicity of primitive cell.

Calorimetric experiments identify three anomalies of heat capacity. Such a situation is in agreement with possible subgroup relations corresponding distortions of pyrochlore structure. The sequence $Fd\bar{3}m \rightarrow I4_1/amd \rightarrow Imma \rightarrow Pnma$ was considered in [15]. Structural transformations in $CsFe_2F_6$ take place in a rather narrow temperature range that make possible the existence in the sample both the temperature gradients and coexisting several phases. This is the reason why the crystal structure of

**Table 4**
Fractional atomic coordinates and isotropic displacement parameters (Å$^2$) of $CsFe_2F_6$ at $T=573$ K and $T=298$ K.

| | $x$ | $y$ | $z$ | $B_{iso}$, Å$^2$ |
|---|---|---|---|---|
| $T=573$ K, $Fd\bar{3}m$ | | | | |
| Cs | 3/8 | 3/8 | 3/8 | 5.29 (6) |
| Fe | 0 | 0 | 0 | 1.72 (6) |
| F | −0.0731 (4) | 1/8 | 1/8 | 3.1 (1) |
| $T=298$ K, *Pnma* | | | | |
| Cs | −0.0117 (3) | 0.25 | 0.37393 (12) | 3.01 (4) |
| Fe1 ($Fe^{III}$) | 0 | 0 | 0 | 1.15 (6) |
| Fe2 ($Fe^{II}$) | 0.7790 (5) | 0.25 | 0.7386 (4) | 1.12 (7) |
| F1 | 0.1500 (8) | 0.9730 (10) | 0.1485 (7) | 1.96 (17) |
| F2 | 0.7184 (9) | 0.4413 (8) | 0.5954 (7) | 1.83 (18) |
| F3 | 0.4601 (14) | 0.25 | 0.4502 (7) | 2.2 (3) |
| F4 | 0.5383 (14) | 0.25 | 0.8223 (8) | 2.1 (3) |

**Table 5**
Main bond lengths of $CsFe_2F_6$ at $T=573$ K and $T=298$ K.

| $T=573$ K, $Fd\bar{3}m$ | | $T=298$ K, *Pnma* | |
|---|---|---|---|
| Bond | length (Å) | Bond | length (Å) |
| Fe–F | 2.012(3) | Fe1–F[i] | 1.902(7) |
| | | Fe1–F2[ii] | 1.920(7) |
| | | Fe1–F3[iii] | 1.963(3) |
| | | Fe2–F1[iv] | 2.106(8) |
| | | Fe2–F2 | 2.113(8) |
| | | Fe2–F4 | 1.95(1) |
| | | Fe2–F4[v] | 1.98(1) |
| Cs–F[x] | 3.175(4) | Cs–F1[i] | 3.345(7) |
| | | Cs–F1[vi] | 3.218(7) |
| | | Cs–F2[vii] | 3.347(7) |
| | | Cs–F3[viii] | 3.385(8) |
| | | Cs–F4[ix] | 3.187(8) |

[i] Symmetry code: $x, y-1, z$.
[ii] Symmetry code: $x+1/2, y-1/2, z-1/2$.
[iii] Symmetry code: $x+1/2, -y, z-1/2$.
[iv] Symmetry code: $x+1, -y+1, -z+1$.
[v] Symmetry code: $x+1/2, -y+1/2, -z+3/2$.
[vi] Symmetry code: $x-1/2, -y+3/2, -z+1/2$.
[vii] Symmetry code: $x-1, y, z$.
[viii] Symmetry code: $x-1/2, -y+1/2, -z+1/2$.
[ix] Symmetry code: $x-1/2, -y+1/2, -z+3/2$.
[x] Symmetry code: $-z+1/2, -x, -y+1/2$.

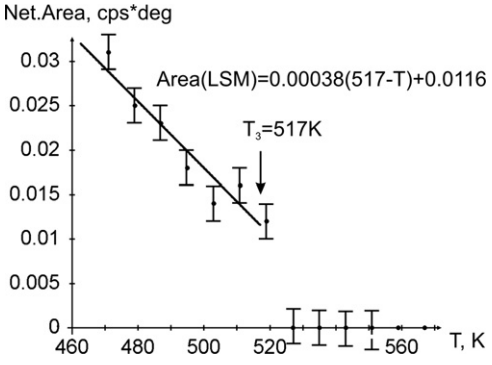


**Fig. 6.** Temperature dependence of the net area of the superstructure peak $(2\ 1\ 0)_{orth}$. Solid line is a result of least square method (LSM) fitting.

intermediate phases could not be solved. The analysis of the appearance of order parameters in this region is difficult. However, splitting of the main reflections as well as superstructure reflections could be pointed out (Figs. 5, 6). One can see that

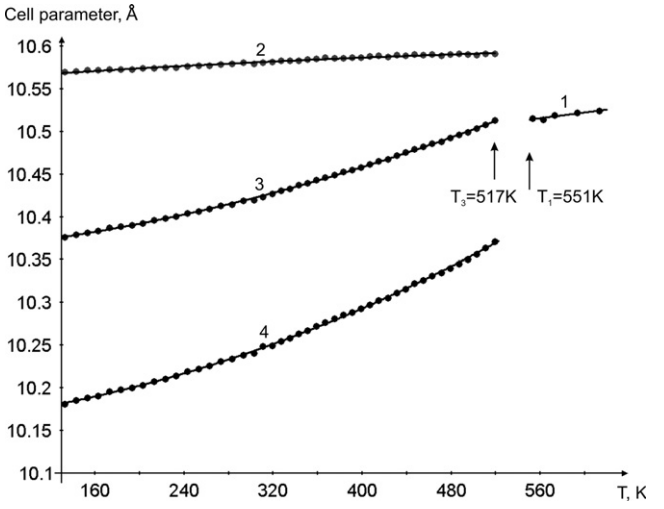


**Fig. 7.** Temperature dependence of the cell parameters: 1—cubic $a_{cub}$; 2—$b_{orth}\sqrt{2}$ 3—$c_{orth}$; 4—$a_{orth}\sqrt{2}$

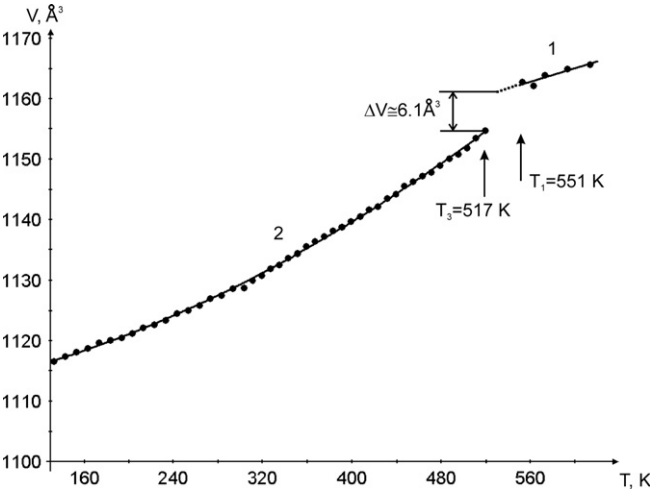


**Fig. 8.** Temperature dependence of the cell volume: 1—cubic phase $V_{cub}$; 2—orthorhombic phase $V_{orth}\times 2$.

splitting appears at $T=551$ K and superstructure peak arises only below $T=517$ K with an increase of the net area on cooling.

So one can conclude that between $T_1=551$ and $T_3=517$ K the order parameters of $GM5+(\xi,0,0)$ and $GM3+(b,0)$ may appear as they do not multiply the primitive cell volume. In this case, intermediate space groups may be the following:

$$Fd\bar{3}m \xrightarrow{(b,0)GM3+} I4_1/amd;\ Fd\bar{3}m \xrightarrow{(\xi,0,0)GM5+} Imma;\ Fd\bar{3}m \xrightarrow{(b,0)GM3+\otimes(\xi,0,0)GM5+} Imma$$

Then below $T_3=517$ K the order parameter $(\eta,0,0,0,0,0)$ of $X4$ arises and phase transition $Fd\bar{3}m \longrightarrow^{(\eta,0,0,0,0,0)X4} Pnma$ is realized. Here order parameters $GM5+(\xi,0,0)$ and $GM3+(b,0)$ are included in $X4$ irrep as noncritical, so their appearance or disappearance does not change space group *Pnma*.

Temperature dependence of the cell parameters and volume are shown in Figs. 7 and 8

## 4. Discussion

The detailed XRD patterns studies have revealed a presence of superlattice reflections in orthorhombic phase of $CsFe_2F_6$ at the room temperature. The symmetry of the Cs compound was

determined as *Pnma* ($Z=4$), as it was found earlier for related fluorides $NH_4Fe_2F_6$ and $RbFe_2F_6$ [18,19].

At the phase transition $Fd\bar{3}m \longrightarrow^{(\eta,0,0,0,0,0)X4} Pnma$ the primitive cell volume is doubled, so one Fe splits on two independent Fe1 and Fe2. Table 5 shows that average $d$(Fe1–F) less than $d$(Fe2–F). Bond valence sum analysis was performed by program PLATON [32]. Program shows that sum bond valency for Fe1 equal to 3.066 and for Fe2 equal to 2.005, so $Fe^{II}$ and $Fe^{III}$ ions occupy Fe2 and Fe1 sites, respectively. *GM*5+ mode leads to such cation ordering $Fe^{II}/Fe^{III}$ in accordance with Mössbauer spectra measured [7]. Complete mode details show that Fe2 ion shifts of 0.107(4) Å and 0.223(4) Å in the $a_{orth}+c_{orth}/2$ and $a_{orth}+c_{orth}$ directions, respectively, driven by *X*4 displacive mode. Overall shift is 0.241(11) Å. Fe1 ions remain at the same position. *GM*5+ drives Cs ions to shift of 0.087(2) Å in the $c_{orth}$ direction. *X*4 mode drives *F* atoms to move in such a way that cluster of five $FeF_6$ octahedra rotates around $b_{orth}$ axis (Fig. 9). The angle of rotation, $\varphi_{1(X4)} \approx 10.4^\circ$, is consistent with angles ranging from 2° to 13.2° quoted for some other related structures with *Pnma* space group [15,30,31]. As one can see in Fig. 9b and c the cluster rotates only around $b_{orth}$. This is evident because both $a_{orth}\sqrt{2}$ and $c_{orth}$ are smaller than $a_{cub}$ (Fig. 7). So, the ($a_{orth}$, $c_{orth}$) face is compressed at phase transition and clusters of octahedral have to rotate. Opposite, $b_{orth}\sqrt{2}$ exceeds the cubic cell $a_{cub}$ parameter and clusters facing ($b_{orth}$, $c_{orth}$) stay unturned. The $\varphi_{1(X4)}$ angle of octahedra rotation can be estimated from the cell parameters. One can see from Fig. 9 that $\cos(\varphi_{1(X4)}) \cong c_{orth}/a_{cub}$, or $\cos(\varphi_{1(X4)}) \cong \sqrt{2}b_{orth}/a_{cub}$. Averaging of both equations and using cell parameters given in Table 2 yields $\varphi_{1(X4)} \cong \arccos(c_{orth}+\sqrt{2}\ b_{orth})/2a_{cub} = 10.7^\circ$. The comparison of measured and calculated rotation angle $\varphi_{1(X4)}$ *at* $T=133$ K gives 12.1° and 12.2°, respectively, (cell parameters at $T=133$ K are $a_{orth}=7.1996(2)$ Å; $b_{orth}=7.4742(2)$ Å, $c_{orth}=10.3765(2)$ Å. Such a good agreement between experimentally found and calculated values allows us to calculate and plot thermal dependence of $\varphi_{1(X4)}$ (Fig. 10), taking into account thermal dependence of the cell parameters (Fig. 7). The angle $\varphi_{1(X4)}$ is directly related to the order parameter $\eta$, and a satisfactory square-root line is obtained. Least-square method confirms a jump $\Delta\varphi_{1(X4)}=6.2^\circ$ at $T_3=517$ K, which accounts for a first-order transition.

As mentioned above, the closeness of phase transition temperatures to each other has prevented us to get information about individual integral characteristics. But rather low value of the total entropy change associated with the succession of three transformations and determined as $\Sigma\Delta S_i = \int(\Delta C_p/T)dT = 2.6 \pm 1.0$ J(mol K)$^{-1}$ shows that structural distortions in $CsFe_2F_6$ are small that indeed was found in X-ray experiments.

The positive change of the unit cell volume of $CsFe_2F_6$ with temperature increase in the region of structural transformations means that the hydrostatic pressure elevates the phase transition temperatures and stabilizes the orthorhombic *Pnma* phase, extending its existence range in temperature.

Table 6 shows the relationship between the changes of the formula unit volume $V_{fu}$ and the symmetry generated by the presence of different $M^{II}$ central atom substitution, or differently by changing chemical pressure in some $AM^{II}Fe^{III}F_6$ compounds.

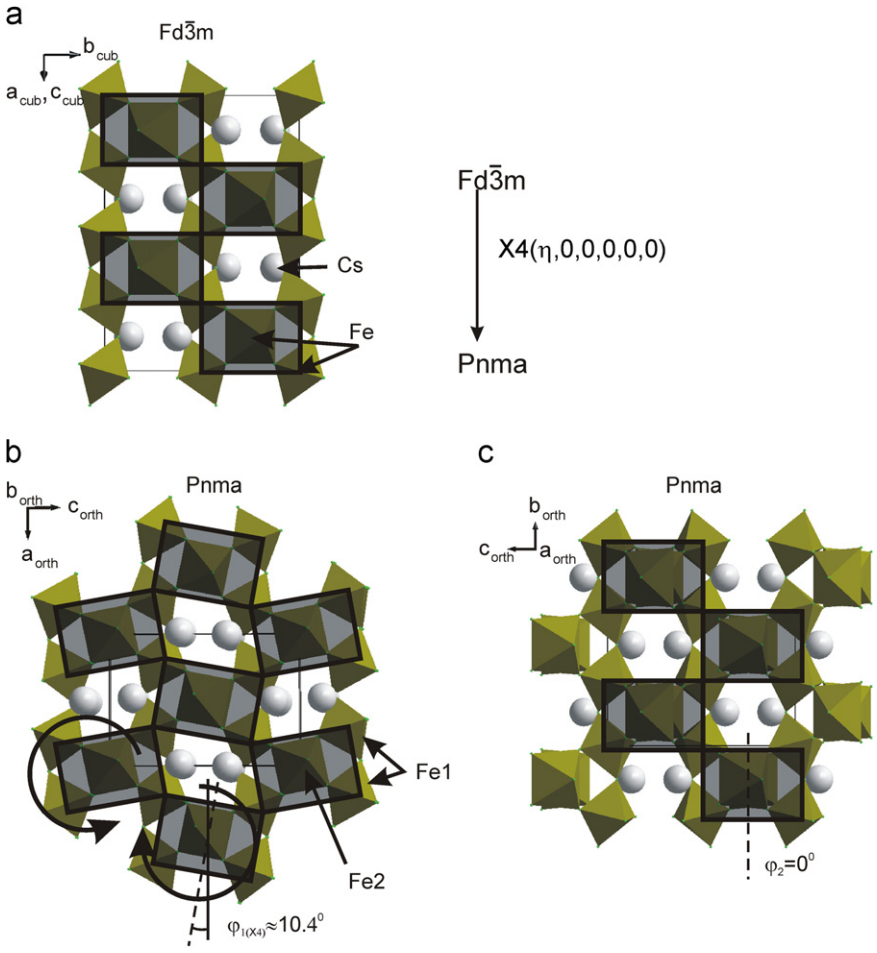


**Fig. 9.** (a) Structure of the cubic phase of $CsFe_2F_6$ at 573 K, grey rectangle—cluster of five $FeF_6$ octahedra; (b) projection on $b_{orth}$ axis of the orthorhombic phase at 298 K, arrows show rotation of $FeF_6$ cluster when order parameter ($\eta$,0,0,0,0,0) of *X*4 appears; (c) projection on $a_{orth}$ axis of the orthorhombic phase, where rotations are absent.

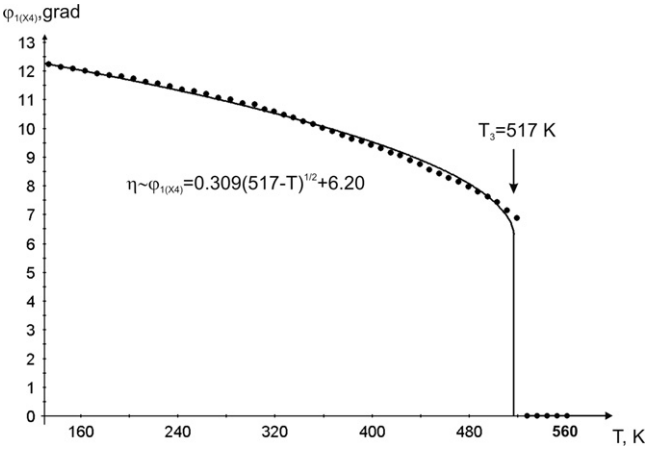


**Fig. 10.** Temperature dependence of $\eta \sim \varphi_{1(X4)}$. Solid line is result of fitting by least square method.

**Table 6**
The formula unit volume $V_{fu}$ and symmetry of some defect pyrochlores $AM^{II}Fe^{III}F_6$. (*RT*—room temperature).

| Compound | *RT* symmetry | $V_{fu}$ (Å$^3$) | Reference | $R_{MII}/R_{Fe3+}$ |
|---|---|---|---|---|
| $CsFeFeF_6$ | *Pnma* | 141.2 | This work | 1.209 |
| $CsAgFeF_6$ | *Pnma* | 146.4 | [30,33] | 1.457 |
| $CsMnFeF_6$ | $Fd\bar{3}m$ | 145.6 | [34] | 1.287 |
| $CsCoFeF_6$ | $Fd\bar{3}m$ | 140.6–141.4 | [8] | 1.155 |
| $CsZnFeF_6$ | $Fd\bar{3}m$ | 140.6 | [8] | 1.147 |
| $CsMgFeF_6$ | $Fd\bar{3}m$ | 137.3–138.2 | [8] | 1.116 |
| $CsNiFeF_6$ | $Fd\bar{3}m$ | 138.6 | [8] | 1.070 |

It can be seen that at room temperature the volume increase is followed by the symmetry decrease from cubic $Fd\bar{3}m$ to orthorhombic *Pnma*. $CsMnFeF_6$ characterized by the anomalous large volume $V_{fu}$, close to that for $CsAgFeF_6$, and $Fd\bar{3}m$ symmetry is an exception to this rule. It is possible to suppose that cubic structure in this compound is metastable as it was observed for $NH_4CoAlF_6$ which showed, depending on the synthesis method, $Fd\bar{3}\ m$ ($V_{fu}$=126.8 Å$^3$) or *Pnma* ($V_{fu}$=124.9 Å$^3$) symmetry [17]. One more example is associated with twofold interpretation of the $CsFeCrF_6$ and $CsFeVF_6$ symmetry on the basis of Mössbauer study. Both compounds were found to be cubic [33] and noncubic [35]. It is also interesting to compare the ionic radii ratio $R_{MeII}/R_{Fe3+}$ (Table 6). The increase of this value leads to stabilization of the orthorhombic phase. For $CsMnFeF_6$ the $R_{MeII}/R_{Fe3+}$ parameter is rather large in comparison to other compounds with $Fd\bar{3}m$ symmetry and close to values characteristic for *Pnma* structure.

## 5. Conclusions

The results of calorimetric and X-ray studies of $CsFe_2F_6$ have shown:

(1) For the first time structural phase transitions induced by the temperature change were found for fluorides $A_xM^{II}_xM^{III}_{(1-x)}F_3$ and $A_xM^{II}_xM'^{III}_{(1-x)}F_3$ with the defect pyrochlore structure ($Fd\bar{3}m$, $Z$=8).
(2) The room temperature structure of $CsFe_2F_6$ is characterized by orthorhombic symmetry (sp. gr. *Pnma*, $Z$=4) with an ordered arrangement of $Fe^{II}$ and $Fe^{III}$ atoms, as in related fluorides $NH_4Fe_2F_6$ and $RbFe_2F_6$.
(3) It was supposed that this structure successively transforms on heating, following the sequence: *Pnma* ($Z$=4)→*Imma* ($Z$=4)→$I4_1/amd$ ($Z$=4)→$Fd\bar{3}m$ ($Z$=8).
(4) In the framework of group-theoretical analysis, the types of the order parameters were found.
(5) This model suggests that the structural distortions are mainly associated with rotation of fluorine octahedra and small displacements of some atoms and is in good agreement with the low experimental entropy value, which is characteristic for displacive transformations.
(6) The increase of the unit cell volume in the phase transitions region accounts for an increase of the existence of *Pnma* phase with temperature under hydrostatic pressure.

## Acknowledgments

This study was supported by the Russian Foundation for Basic Research, project no. 12-02-00056, and Grant NSh-4828.2012.2 of the President of the Russian Federation for the Support of Leading Scientific Schools.

## References

[1] P. Hagenmüller (Ed.), Academic Press, 1985, City.
[2] I.N. Flerov, M.V. Gorev, K.S. Aleksandrov, A. Tressaud, J. Grannec, M. Couzi, Mater. Sci. Eng. R24 (3) (1998) 81–151.
[3] J. Ravez, S. Arquis, J. Grannec, J. Appl. Phys. 62 (1987) 4299–4301.
[4] D. Babel, G. Pausewang, W. Viehahn., Z. Naturforsch. 22b (1967) 1219–1225.
[5] D. Babel, F. Binder, G. Pausewang, Z. Naturforsch. 28b (1973) 213–215.
[6] J.L Fourquet, C. Jacoboni, R. de Pape, Mat. Res. Bull. 8 (1973) 393–404.
[7] N.N. Greenwood, F. Menil, A. Tressaud, J. Solid State Chem. 5 (1972) 402–409.
[8] B.M. Wanklyn, F.R. Wondre, B.J. Garrard, J. Cermak, W. Davison, J. Mater. Sci. 16 (1981) 2303–2309.
[9] I.N. Flerov, M.V. Gorev, A. Tressaud, N.M. Laptash, Crystallogr. Rep. 56 (2011) 9–17.
[10] A. Tressaud, R. de Pape, J. Portier, P. Hagenmüller, Bull. Soc. Chim. Fr. 10 (1970) 3411–3413.
[11] D. Paus, R. Hoppe, Z. Anorg. Allg. Chem. 426 (1976) 83–94.
[12] A. Tressaud, F. Ménil, R. Georges, J. Portier, P. Hagenmüller, Mater. Res. Bull. 7 (1972) 1339–1346.
[13] J. Ravez, S.C. Abrahams, R. de Pape, J. Appl. Phys. 65 (1989) 3987.
[14] F. Mezzardi, S. Fabbrici, E. Montanari, L. Righi, G. Calestani, E. Gilioli, F. Bolzoni, A. Migliori, Phys. Rev. B 78 (2008) 064111.
[15] A. Grzechnik, W. Morgenroth, K. Friese, J. Solid State Chem. 182 (2009) 1792–1797.
[16] D. Babel, Z. Anorg. Allg. Chem. 387 (1972) 161–178.
[17] M.A. Subramanian, W.J. Marshall, R.L. Harlow, Mater Res. Bull. 31 (1996) 585–591.
[18] G. Ferey, M. Leblanc, R. de Pape, J. Solid State Chem. 40 (1981) 1–7.
[19] S.W. Kim, S.-H. Kim, P.S. Halasyamani, M.A. Green, K.P. Bhatti, C. Leighton, H. Das, C.J. Fennied, Chem. Sci. 3 (2012) 741–751.
[20] E. Baum, P. Dahlke, V. Kaiser, M. Molinier, R.E. Schmidt, J. Pebler, W. Massa, D. Babel, Z. Anorg. Allg. Chem. 632 (2006) 2244–2250.
[21] I.C. Madsen, R.J. Hill, Adv. X-ray Anal. 35 (1992) 39–47.
[22] I.C. Madsen, R.J. Hill, J. Appl. Cryst. 27 (1994) 385–392.
[23] W.I.F. David, Abstract P2.6, NIST Special Publication, 846, NIST, 1992, p. 210.
[24] Diffrac-Plus Basic XRD Wizard. 2002–2007 Bruker AXS GmbH, Karlsruhe, Germany.
[25] W.I.F. David, K. Shankland, J. van de Streek, E. Pidcock, W.P.S. Motherwell, J.C. Cole, J. Appl. Cryst. 39 (2006) 910–915.
[26] Bruker AXS (2008): TOPAS V4: General Profile and Structure Analysis Software for Powder Diffraction Data.—User's Manual, Bruker AXS, Karlsruhe, Germany.
[27] V.I. Mikheev. X-ray identification of minerals. M: Geology and Protection of Natural Resources, 1957.
[28] H.T. Stokes, D.M. Hatch, B.J. Campbell. ISOTROPY (2007) stokes.byu.edu/isotropy.html.
[29] B.J. Campbell, H.T. Stokes, D.E. Tanner, D.M. Hatch, J. Appl. Crystal. 39 (2006) 607.
[30] B.G. Müller, J. Fluor. Chem. 17 (1981) 317–329.
[31] K. Friese, J.Y. Gesland, A. Grzechnik, Z. Kristallogr. 220 (2005) 614–621.
[32] PLATON (2008): A Multipurpose Crystallographic Tool. Utrecht University, Utrecht, The Netherlands.
[33] W. Grochala, R. Hoffmann, Angew. Chem. Int. Ed. 40 (2001) 2742–2781.
[34] E. Banks, J.A. Deluca, O. Berkooz, J. Solid State Chem. 6 (1973) 569–573.
[35] Y. Calage, F. Varret, Chem. Phys. Lett. 55 (1978) 380–382.